Catalytic modification of conventional SOFC anodes with a view to reducing their activity for direct internal reforming of natural gas

M. Boder, R. Dittmeyer*

Research Group Technical Chemistry, Karl-Winnacker-Institut, DECHEMA e.V., Theodor-Heuss-Allee 25, D-60486 Frankfurt, Germany

Abstract

When using natural gas as fuel for the solid oxide fuel cell (SOFC), direct internal reforming lowers the requirement for cell cooling and, theoretically, offers advantages with respect to capital cost and efficiency. The high metal content of a nickel/zirconia anode and the high temperature, however, cause the endothermic reforming reaction to take place very fast. The resulting drop of temperature at the inlet produces thermal stresses, which may lower the system efficiency and limit the stack lifetime. To reduce the reforming rate without lowering the electrochemical activity of the cell, a wet impregnation procedure for modifying conventional cermets by coverage with a less active metal was developed. As the coating material copper was chosen. Copper is affordable, catalytically inert for the reforming reaction and exhibits excellent electronic conductivity. The current density–voltage characteristics of the modified units showed that it is possible to maintain a good electrochemical performance of the cells despite the catalytic modification. A copper to nickel ratio of 1:3 resulted in a strong diminution of the catalytic reaction rate. This indicates that the modification could be a promising method to improve the performance of solid oxide fuel cells with direct internal reforming of hydrocarbons.
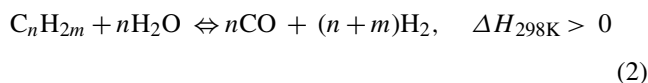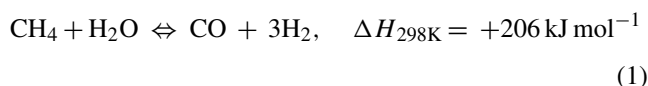© 2005 Elsevier B.V. All rights reserved.

Keywords: Steam reforming; Internal reforming; Solid oxide fuel cell; Nickel/zirconia anode; Copper; Wet impregnation
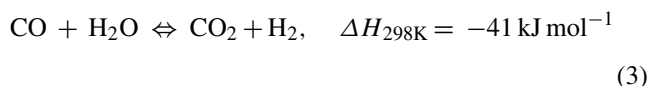
1. Introduction

One great advantage of the solid oxide fuel cell (SOFC) compared to other fuel cells is that – in principle – hydrocarbons can be converted directly. Therefore, the SOFC could be put into operation right away within the existing energy infrastructure. Once hydrogen becomes readily available, the SOFC can be switched to hydrogen operation mode quite easily. Given the existence of a widespread distribution network, natural gas is presently the fuel of choice for the SOFC. However, the addition of steam is necessary to generate a hydrogen-rich gas by the so-called steam reforming reaction, which in current SOFC installations mainly takes place over a ceramic-supported nickel catalyst in a pre-reformer unit [1,2]. The process involves the following reactions:

Steam reforming:

$$CH_4 + H_2O \Leftrightarrow CO + 3H_2, \quad \Delta H_{298K} = +206 \, \text{kJ mol}^{-1} \tag{1}$$

$$C_nH_{2m} + nH_2O \Leftrightarrow nCO + (n+m)H_2, \quad \Delta H_{298K} > 0 \tag{2}$$

Water gas shift:

$$CO + H_2O \Leftrightarrow CO_2 + H_2, \quad \Delta H_{298K} = -41 \, \text{kJ mol}^{-1} \tag{3}$$

Using the Ni–YSZ anode as catalyst and converting the hydrocarbons directly in the anode compartment simplifies the whole system and, theoretically, offers advantages with respect to capital cost. It lowers the requirement for cell cooling and consequently less excess air is needed. Under practical conditions up to half of the heat produced by the

exothermic oxidation reactions could be dissipated by the reforming processes. This would also improve the electrical efficiency of the entire system. Moreover, there is an increase in system efficiency by eliminating the energy penalty associated with transferring the heat for reforming to an external reformer [3,4].

The high nickel content of the conventional anode, which typically is around 50 vol.% and the high temperature of up to about 950 °C, however, cause the endothermic reforming reaction to take place very fast. Therefore, complete internal reforming leads to a large temperature drop at the inlet of the stack. The consequence is a decrease in efficiency due to erasure of the electrochemical reactions. In other areas oxidation reactions take place at high temperatures. The temperature gradients result in tensions which can possibly cause leakage and, in the worst case, mechanical failure of the cell. For a reliable operation the reforming rate has to be adapted to the rate of the oxidation reactions.

To minimize the drawbacks of entire internal reforming different alternatives are conceivable.

1.1. External or integrated (=indirect internal) reforming

A significant temperature drop can be avoided if the hydrocarbons are partly converted prior to entering the anode compartment. This could be done in a completely separated external or in an integrated reformer unit. The second possibility involves a reforming catalyst which is in close thermal contact with, but spatially separated from, the fuel cell stack. This leads to a fuel gas that already contains significant amounts of hydrogen and carbon monoxide. State-of-the-art fuel cell systems contain a partial pre-reforming step with about 30–50% conversion ahead of the fuel cell [2]. However, the idea is to save this process step mainly because of cost-saving reasons.

1.2. Chemical engineering measures

A partial recycling of the anode gas leads to a dilution of the fuel. The concentration distribution along the cell becomes more even and the reforming rate decreases due to the reduced concentration of the hydrocarbon fuel. This results in a more uniform temperature and current density distribution. Referring to the whole system, the fuel utilisation increases. If about half of the anode gas is recycled, there is enough steam from the oxidation available for the reforming process. Hence, the expenditure for a separate water supply could be saved [5,6].

The flow guidance of the gases within the stack can influence the magnitude of the cooling. With planar cells, the smallest temperature gradients occur when the fuel gas and the air flow concurrently [3].

Another technique is to admit the fuel in stages along the cell. This is more easy to achieve with tubular cells and has been applied by Westinghouse [7].

The construction design of the stack can also have a considerable influence on the local decrease of current density. Optimising the heat exchange by the use of suitable casing materials as well as the design of the cell interconnect leads to smaller temperature gradients and therefore, to an advantageous current distribution [8].

1.3. Application of alternative anode materials

A further method is to design an alternative anode material with lower steam reforming activity. A great deal of the research carried out at present concentrates upon the search for single-phase ceramic oxides which exhibit lower catalytic activity. However, up to now the electronic conductivity of these materials is still too low to meet the requirements of practical devices [9,10].

1.4. Modification of the Ni–YSZ cermets

During the fabrication process nickel can be replaced by a less catalytically active metal, for instance, iron. Morimoto and Shimotsu [11] showed that the thermal expansion of a Fe–YSZ cermet can be adapted to that of the solid electrolyte. However, the stability of iron depends strongly on the oxygen partial pressure [12]. Thus, an entire substitution of nickel is doubtful. An effective measure to reduce the catalytic activity could be a partial substitution of nickel by iron.

The state-of-the art Ni–YSZ cermets have been optimised for the application of hydrogen as fuel. A promising method with respect to short-term technical application is the modification of these standard materials with a view to lowering their reforming activity. An important advantage of this approach is based on the fact that the well-established production process for the cells could be maintained.

Planar cells with a self supporting electrolyte served as the standard material for the investigations described in this paper. In order to lower the catalytic activity a procedure was developed which enables partial covering of the active nickel surface sites. As the coating material copper was chosen. Copper is an excellent electrical conductor; hence, it should be possible to maintain the electrochemical performance of the standard cells with unmodified anodes. The reactivity of nickel for the hydrogenolysis as well as for hydrogenation and dehydrogenation is altered by alloy formation with copper. These reactions are also of crucial importance for the deactivation by coking. In 1972 Sinfelt et al. [13] examined the production of methane out of ethane and hydrogen. This reaction involves rupture of C−C bonds and is representative of a fragmentation reaction of hydrocarbons on metals. They observed that the hydrogenolysis activity of nickel-containing catalysts declines by five orders of magnitude when the copper content is increased from 0 to 60%. Unlike most other transition metals copper is also regarded as relatively inert for the formation of C−C bonds. Bernardo et al. [14] added copper to nickel containing catalysts in order to improve their coking resistance. Apart from decreasing coke

formation, the activity for the steam reforming reaction also diminished strongly with rising copper content. Hegarty et al. [15] compared different ZrO_2-supported catalysts (1 mass% metal) regarding their activity for synthesis gas production in the temperature range of 400–800 °C. The use of copper containing catalysts led to very small methane conversion rates. Copper promotes the activation and the decomposition of water and has a negligible activity for the dissociation of methane. Thus, the effectiveness regarding the reforming reaction is small, while the shift reaction is catalysed. Moreover, it is also relatively inexpensive [16,17].

2. Experimental

2.1. Experimental set-up for solid oxide fuel cell investigation

The SOFC experimental facility is a test unit for a single cell (Fig. 1). It consists basically of four main parts: (1) gas dosing and humidification, (2) the fuel cell itself, (3) a sampling device and a unit for the analysis of the exhaust gases and (4) measurement and control of current and voltage.

(1) Mass flow controllers from Brooks Instrument regulate the inlet gas flows of hydrogen, argon and/or methane on the anode and air on the cathode side. A membrane humidifier is used to adjust the required water content of the fuel. All pipes and valves between humidifier, furnace and the condensers are heated to prevent condensation of water.

(2) The fuel cell is placed in a ceramic casing, which consists of three separate parts made of alumina. The casing built by Wesgo basically supports the cell, assures a tight connection between the electrodes and the metal nets needed for the electric contact, guarantees the sealing of the electrode compartments and enables the feeding and removal of the gas streams. A gold ring on each side of the solid electrolyte acts as sealing material. In addition there are two alumina frames between the gold rings and the casing parts which seal the electrode compartments against the outside atmosphere. As thermal self-preservation is not possible with one single cell, the ceramic reactor is situated in a chamber oven which allows a maximum temperature of 1100 °C.

(3) For the analysis part of the anode, waste gas (<10 vol.%) is separated from the main exhaust. The water content of this smaller stream is continuously determined by a dew point hygrometer. After that the analysis stream is dried by condensation of the water to less than 1% of absolute humidity. Finally a gas chromatograph ascertains the concentrations of the remaining components (methane, hydrogen, carbon monoxide and carbon dioxide) in the dry gas within defined time intervals. The mass balance calculated for each measurement proved that other species occur only in trace amounts.

(4) The electric contact of the electrodes must guarantee good access of the gas to the electrodes and should preferably be reusable. Therefore, metallic nets, platinum on the cathode and nickel on the anode side, were used. Mechanical pressing with weights guarantees a tight contact all over the electrode area. The influence of the wire
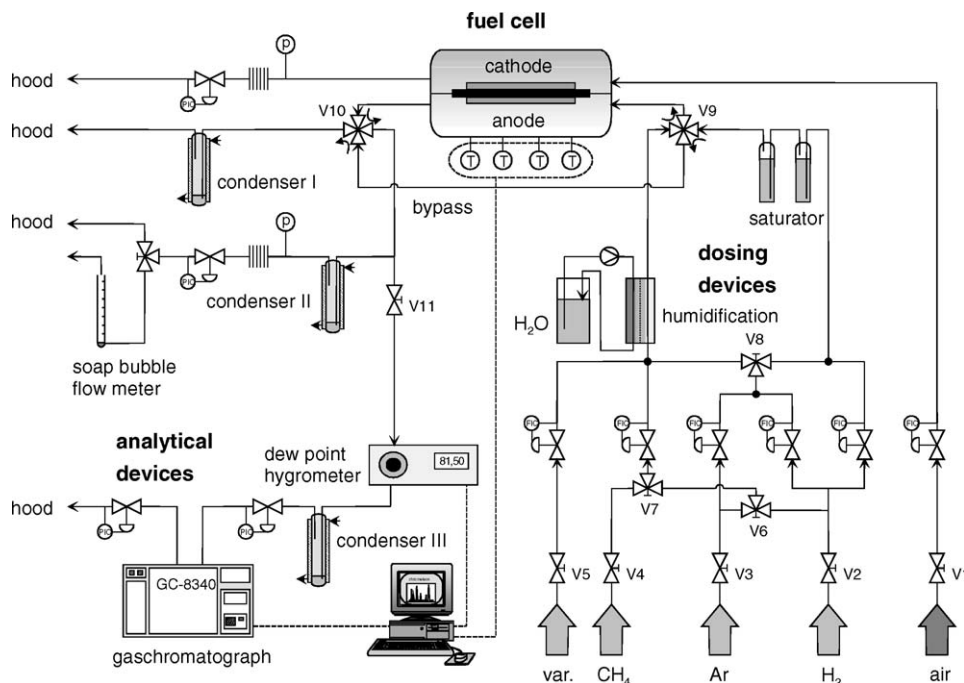

Fig. 1. Experimental set-up for the investigation of internal steam reforming of methane in a solid oxide fuel cell.
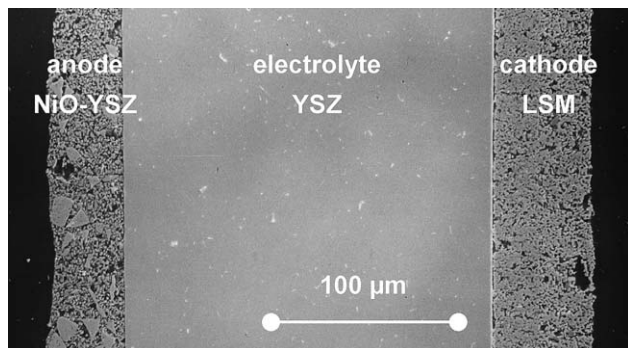
Fig. 2. SEM micrograph showing a cross section of the deployed standard cell.

resistances is eliminated by a 4-pole contact of the cell. A D/A converter enables the adjustment of the current and A/D converters are used to save the measured values of current and voltage on a personal computer. A special program written with the visual programming language LabView is used to execute the necessary steps and record the attained results.

2.2. Features of the standard cell

2.2.1. Composition and structure

The electrolyte of the standard cells used for the investigations was a planar square out of 8YSZ (8 mol% Y_2O_3–stabilized ZrO_2) with a thickness of 200 μm. The ceramic sheet acted as a substrate for the screen printing of the electrode layers carried out by our cooperation partner Siemens. In Fig. 2 a scanning electron micrograph (SEM) showing a cross section of the standard cell can be seen. The cathode material used was Sr-doped lanthanum manganite. There were two different layers having an overall thickness of about 50 μm. The one close to the electrolyte contained a certain amount of YSZ and had a higher porosity than the outer layer. The anode was approximately 40 μm thick and consisted of Ni–8YSZ. It was manufactured by a coat mix process starting with a powder mixture of NiO and 8YSZ together with a binder. The cermet was reduced at 950 °C in a hydrogen/argon mixture with a gradually increasing partial pressure of hydrogen. After the reduction it contained about 65 wt.% nickel. The geometric electrode area of each cell was 9×10^{-4} m^2 (3 cm × 3 cm).

2.2.2. Surface area of the anode material

For the determination of the specific surface area of the anode material the BET method was used. The measurements were performed with a Sorptomatic 1990 from Thermo Electron Corporation.

The experiments revealed a total surface area of around 2.0 m^2 g^{-1} for NiO/YSZ and 4.4 m^2 g^{-1} for Ni/YSZ. The surface area grows with the reduction because the nickel particles are smaller than the NiO particles and therefore more channels in the anode structure become available for the gas.

2.2.3. Catalytically active nickel area

Metallic nickel serves as a catalyst for the steam reforming reaction on the anode. Therefore, the nickel surface area is interesting when dealing with the heterogeneously catalysed reaction. For the estimation of this important value a titration method was used where a chemisorbed gas is titrated by reaction with another gas. For nickel the titration of adsorbed oxygen with hydrogen is suitable to determine the surface. The advantage of this method lies in the fact that an accurately defined state is created by the specific oxidation of the surface nickel. Therefore, oxygen (for instance from inert gas used for cleaning the pipes) cannot falsify the results.

The nickel surface of the sample is covered entirely with oxygen by pulsing with an oxygen/helium mixture. Subsequently the pre-treated powdery sample (approximately 0.3 g) is heated in a hydrogen/argon atmosphere up to 400 °C. From the hydrogen consumption ascertained with a thermal conductivity detector, the oxygen loading can be calculated. If an oxygen molecule adsorbs dissociatively on two nickel atoms, one hydrogen molecule is used to produce one molecule of water per nickel atom. Therefore, the resulting stoichiometric factor is one. The measurements were carried out with a Porotec TPD/R/O 1100 instrument.

The nickel surface area of the reduced anode material determined by the titration method was 1.2 m^2 g^{-1}. This means that the metal surface area amounts to approximately 30% of the BET surface area. The identified value agrees well with other published results that range from 0.35 to 3 m^2 g^{-1} [18,19].

2.2.4. Electrochemical performance

To quantify the electrochemical performance, current density–voltage characteristics were measured. The open-circuit voltage of the cell corresponds well to the theoretical cell voltage predicted by the Nernst equation. As current is progressively drawn the cell voltage falls as power is dissipated in internal resistances. The measurement of the current density–voltage curves is done galvanostatically. It starts without load; every minute the current is raised by 0.1125 A and kept constant until the next increase. The cell voltage is measured every 10 s. To prevent damage of the cells, the current increase is stopped when the cell voltage reaches 0.6 V. As the normal maximum sustained power point for an SOFC is in the region of 0.7 V per cell lower voltages are not interesting from a technical point of view. Generally this measurement is repeated at least once before the intended experimental program is started. The current density–voltage curves for four different temperatures can be seen in Fig. 3. Within the examined range of up to 0.8 A cm^{-2} the voltage decreases linearly with rising current density. Therefore, the cell resistance can be determined by calculating the slope of the curve. With hydrogen/water mixtures (50 mol% H_2O) and air, the standard cell showed an inner resistance of about 0.36 Ω cm^2 at 950 °C and 0.73 Ω cm^2 at 850 °C.

The quality of the current density–voltage curves shows that the described experimental set-up works well and is suffi-
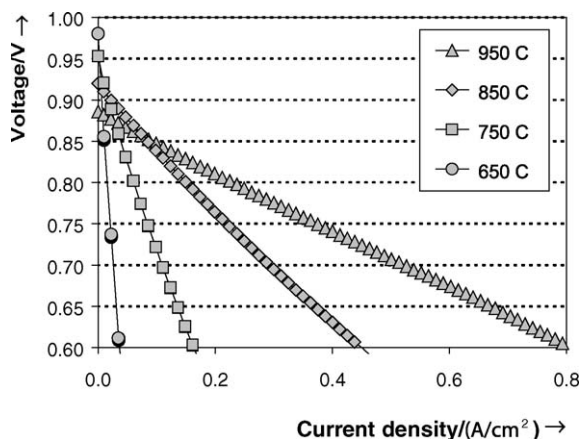
Fig. 3. Current density–voltage relationships of a solid oxide fuel cell using a Ni/YSZ cermet at different temperatures. Anode: $\dot{V}_{0,H_2,SATP} = 181\,h^{-1}$, $x_{0,H_2O} = 0.5$; cathode: air.

ciently leak tight. The results also guarantee that the standard cells are suitable as a reference for the investigation of the catalytically modified cells.

2.3. Coating of the anode with copper

In order to lower the catalytic activity of the described anode material a procedure was developed which enables partial covering of the active nickel surface sites. As the coating material copper was chosen due to its low price, catalytic inertness and excellent electronic conductivity as outlined earlier. However, the melting temperature of copper is rather low (1083 °C). Therefore, to maintain the well-established cell manufacturing process, which requires temperatures up to 1250 °C, copper was applied to the ready-made anodes afterwards.

For this purpose a wet impregnation procedure with aqueous solutions of $Cu(NO_3)_2$ was developed. A slow deposition in a dry cupboard where the temperature can be kept constant steadily allows a uniform copper distribution throughout the anode material. For improving the deposition process the solution was heated to 95 °C and a small amount of solution was used. Thus, a reasonable part of the liquid evaporated and

part of the copper nitrate precipitated. This effect is intensified by the addition of sodium hydroxide. After the impregnation a calcination step followed to decompose the nitrate and to form the oxide. For higher copper concentrations the whole procedure was repeated up to three times.

The global distribution of copper within the anode was determined by microanalysis with a Cameca SX50 electron microprobe (EPMA, electron micro probe analysis). This instrument is a type of scanning electron microscope specially built for chemical analysis using wavelength dispersive spectrometers (WDS) to detect and measure the X-rays generated by an electron beam hitting the sample. The microstructure is characterized by a combination of secondary and back-scattered electron imaging and X-rays elemental mapping. The detectors are capable of detecting elements from Boron to Uranium, at concentrations above about 0.5 mass%.

Instrumental calibration is carried out using standard reference materials. A comparison allows the quantification of the chemical composition of an unknown sample in the micrometer range. The distribution of an element along a line can be determined by scanning across a specimen. For accurate EPMA analysis it is necessary for the specimen to be conductive, flat and well polished, presented perpendicular to the electron beam and clean. The samples are mounted in a resin, polished and cleaned. After that non-conducting samples must be coated by carbon or by a metal. For the investigation of the composition throughout the depth of the anode, a cross section is necessary.

Fig. 4 shows a SEM photograph of the anode (backscattered mode) together with the copper distribution acquired by WDS. The images demonstrate that the inhomogeneous structure of the anode leads to a non-uniform coating throughout the depth of the anode. Although there are areas of higher and lower concentration, no dependence on the depth inside the anode layer is observable.

For the quantitative analysis of the copper concentration every specimen was examined by WDS in at least three series of measurements. Throughout the anode thickness, equidistant measuring points were investigated. The beam diameter of the instrument is approximately 3 μm, the penetration depth is also around 3 μm. Fig. 5 shows exemplarily the mass
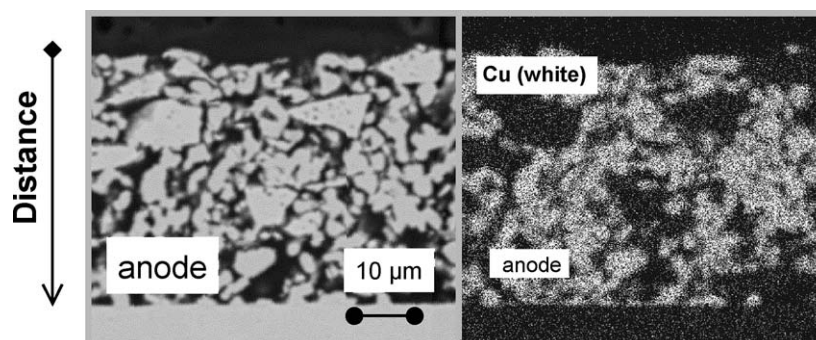

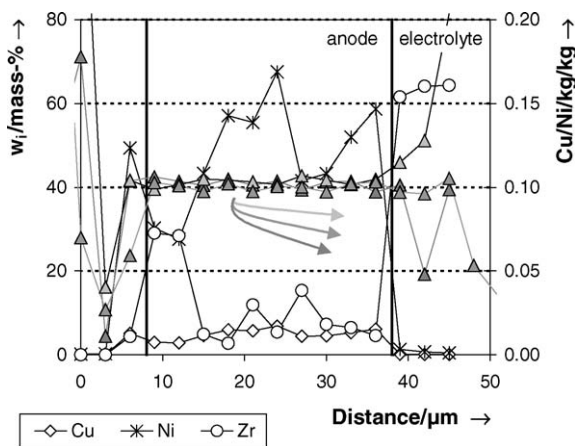Fig. 4. Ni/YSZ cermet: SEM picture and WDS of copper.

Fig. 5. Distribution of copper throughout the depth of the reduced anode material. The ratio of nickel to copper (filled triangles) is constant throughout the anode layer.

Fig. 7. Current density–voltage relationships for a temperature of 950 °C. Performance of the standard unit compared to cells with catalytically modified anode materials. Anode: $\dot{V}_{0,CH_4,SATP} = 17,641\,h^{-1}$, $\dot{n}_{0,H_2O}/\dot{n}_{0,CH_4} = 2$, $x_{0,H_2} = 0.02$; cathode:air.

fractions of nickel, zirconium and copper at one measuring point. The inhomogeneities cause heavily fluctuating concentrations. Due to the voids induced by the porosity of the anode the sum of the ascertained fractions does not necessarily add up to 100%. The mass ratio of copper to nickel, however, remains constant throughout the depth of the anode. Three different series of measurements are shown in Fig. 5. They demonstrate that the amount of copper is directly related to the nickel content.

For the electrode area deviations of the ratio of nickel to copper from the average value were in the range of ±10%. As can be seen from Fig. 6 the ratio of copper to nickel was proportional to the duration of the impregnation process. The copper content could be controlled by the operation parameters during the deposition process, mainly the concentration of $Cu(NO_3)_2$, and the duration. The maximum copper to nickel ratio is in the range of 0.3–0.5 kg kg^{-1}.
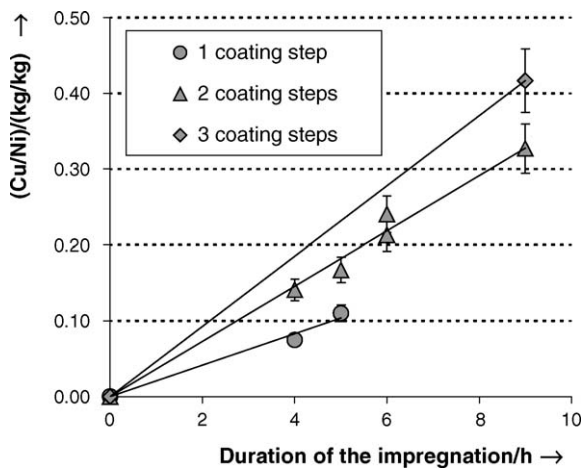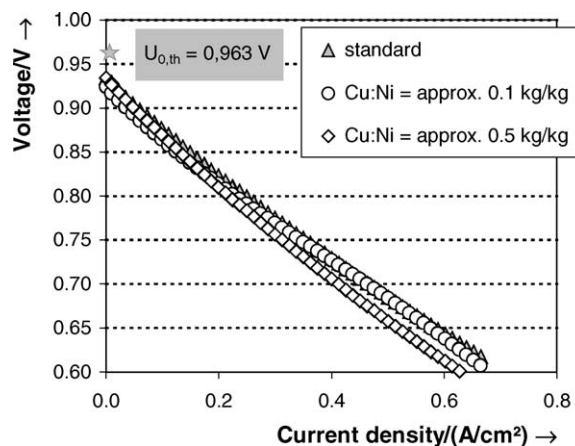
3. Results and discussion

3.1. Electrochemical performance of the modified cells

Two cells with different copper concentrations in the anode were compared electrochemically with the standard unit, one with a ratio of 0.1 kg$_{Cu}$ kg$_{Ni}$$^{-1}$ and the other with a ratio of 0.5 kg$_{Cu}$ kg$_{Ni}$$^{-1}$. When a hydrogen/water mixture (50 mol% H_2O) was used as fuel (cathode:air) the cells showed only a slightly higher inner resistance of 0.42 Ω cm^2 at 950 °C than the standard cell (cf. Fig. 3). Fig. 7 gives the current density–voltage characteristics measured with methane as fuel. The inlet stream of the anode consisted of methane and water at a molar ratio of 0.5 and 2 mol% hydrogen. The measured open-circuit voltage is similar for all three cells. However, it is smaller than the theoretical value. This can be attributed to the fact that contrary to the assumptions made for the calculation of the theoretical value, the anode reactions are not in thermodynamic equilibrium (over the entire anode surface area) under open-circuit conditions. For the standard cell the total polarization resistance amounts to approximately 0.48 Ω cm^2 at 950 °C. As already observed for hydrogen operation mode, the inner resistance of the two catalytically modified cells is also only slightly higher than the resistance of the standard cell.

The current density–voltage characteristics of the modified units show that it is possible to maintain the electrochemical performance of the cells despite the anode modification by copper deposition. In both modes, i.e. with hydrogen and with methane, the total cell resistance increases only slightly. Thus, it is assumed that the internal resistance of the anode is almost independent of the copper content in the concentration range of 0.1–0.5 kg$_{Cu}$ kg$_{Ni}$$^{-1}$. Despite the impregnation with copper a sufficient electrochemical activity of the cells is ensured.

Fig. 6. Dependency of the deposited copper amount on the duration of the impregnation process; concentration: 200 g l^{-1} $Cu(NO_3)_2$, temperature: 95 °C, calciniation: 380 °C, 3 h.

3.2. Internal reforming activity of the modified anode materials

The comparison of the reforming activity was based on measurements without load to avoid an influence of the nickel mesh used to contact the anode when there was a current flow. The pseudo-homogeneous one-dimensional model of the plug flow reactor was applied to describe the concentration profiles which occur in the flow channels above the anode. Temperature and pressure were assumed to be constant throughout the whole anode compartment, concentration gradients transversely to the flow direction were considered negligible. Only convective transport was taken into account while axial dispersion was neglected. The ideal gas law was employed to account for the changing linear gas velocity along the reactor length due to the volume change caused by the chemical reactions. This leads to the following system of ordinary differential equations which were solved to describe the partial pressure profile along the direction of flow:

$$\frac{\partial p_i}{\partial z} = -p_i \frac{RT}{pu} \sum_j \sum_k v_{kj} r_j + \frac{RT}{u} \sum_j v_{ij} r_j \tag{4}$$

We found that the data obtained in the temperature range of 650–950 °C could be well described by a simple kinetic model considering only the reforming and the shift reaction. The model assumes the following reaction rates as basis for the mass balance:

Steam reforming:

$$r_1 = k'_{0,1} \exp\left(\frac{-E_{A,1}}{RT}\right) p_{CH_4}\left(1 - \frac{p_{CO} p_{H_2}^3}{p_{H_2O} p_{CH_4} K_{p,1}}\right) \tag{5}$$

Water gas shift:

$$r_2 = k'_{0,2} \exp\left(\frac{-E_{A,2}}{RT}\right) p_{CO}\left(1 - \frac{p_{CO_2} p_{H_2}}{p_{H_2O} p_{CO} K_{p,2}}\right) \tag{6}$$

For the steam reforming reaction the reaction quotient is very small, i.e. the reforming reaction is sufficiently far from thermodynamic equilibrium for all conditions investigated. The water gas shift reaction, however, is quite close to equilibrium. Therefore, the expression in brackets becomes close to zero. For the comparison of the kinetic properties of modified and unmodified anode materials effective reaction rate constants were used. Unlike the $k'_{0,i}$, which are based on the pseudo-homogeneous reactor volume, the frequency factors $k_{0,i}$ were related to the geometric area of the anode:

$$k_{0,j} = k'_{0,j} \frac{V_R}{A} \tag{7}$$

The non-linearity of the Arrhenius law is known to impede significantly the estimation of parameters by regression. This is caused by an artificial linear correlation between the frequency factor and the activation energy arising from nearly parallel directions of the partial derivatives of the objective function with respect to the two parameters (parameter effects non-linearity). As a consequence the confidence region for the parameter estimates usually derived from a linearization of the model is extremely deformed and does not provide a reasonable measure for the quality of the parameter estimates. To avoid these problems the regression method employed uses the following transformation to render the partial derivatives of the objective function with respect to the new parameters more orthogonal:

$$k_j^* = \ln(k_{0,j}(\text{mol}^{-1}\,\text{m}^{-3}\,\text{Pa}^{-1}\,\text{s}^{-1})) - \frac{E_{A,j}}{RT_R} \tag{8}$$

$$E_j^* = \frac{E_{A,j}}{RT_R} \tag{9}$$

The reference temperature T_R should be chosen in the middle of the temperature interval of interest and was set here to 1073 K. Another numerical advantage of this transformation is that the order of magnitude of all k_j^* is similar and that k_j^* can never become negative during execution of the regression algorithm, which improves convergence.

By application of the pseudo-homogeneous plug flow reactor model and the regression method outlined above, kinetic constants $k_{0,i}$ and $E_{A,i}$ were derived from the concentrations measured at the outlet of the fuel cell for known experimental conditions (inlet concentrations, temperature, pressure, etc.). Fig. 8 illustrates the findings for the described standard anode material. It shows the partial pressures of methane (a) and hydrogen (b) as a function of the residence time within the anode compartment for a temperature range of 650–950 °C. The experimental results are compared to the profiles calculated by the model based on the two reaction rate laws given above. The measured values are well described by this simple kinetic model. It has to be mentioned that apart from the temperature only the contact time on the anode, i.e. the flow rate was varied. The influence of different feed compositions on the reaction rate was not studied. Instead it was assumed that a formal power law could describe the concentration dependency according to the reaction stoichiometry. The kinetic parameters, which were gained without the presence of nickel nets in the anode compartment, in the following serve as basis for the comparison of the standard Ni–YSZ cermets with the catalytically modified anodes.

For the anodes that had been impregnated with copper measurements analogue the standard unit were carried out. Table 1 lists the estimates for the transformed parameters together with the corresponding confidence intervals. The kinetic constants of the reforming reaction for different modified anode materials are compared to the standard anodes. As can be seen from this table, a higher copper content in the cermet generally leads to a lower reforming activity. Moreover, the activation energy clearly increases when the copper content is raised. Therefore, the inhibition effect is even stronger at lower temperatures. For a temperature of 950 °C, a copper to nickel ratio of 1:3 leads to the decrease of the catalytic
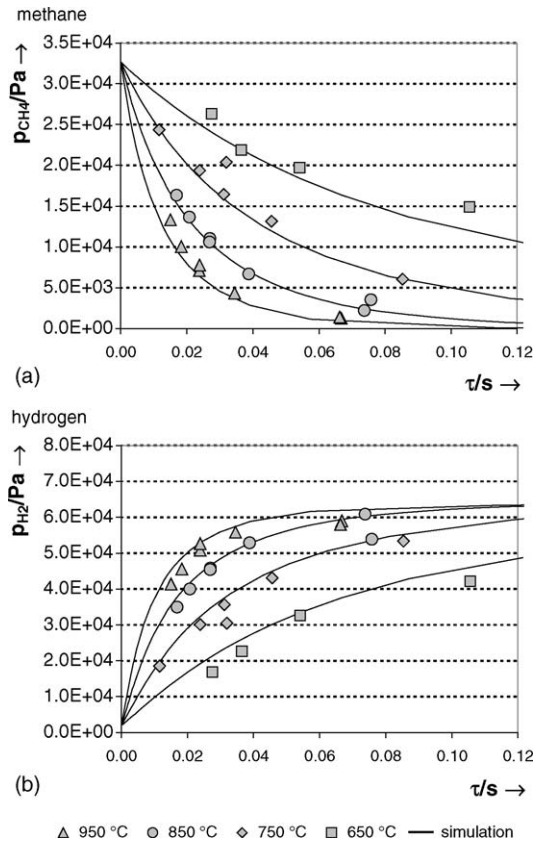
Fig. 8. Partial pressures of methane (a) and hydrogen (b) as a function of the mean residence time. Comparison of measured and simulated values. Anode: $x_{0,CH_4} = 0.33$; $x_{0,H_2O} = 0.65$; $x_{0,H_2} = 0.02$.
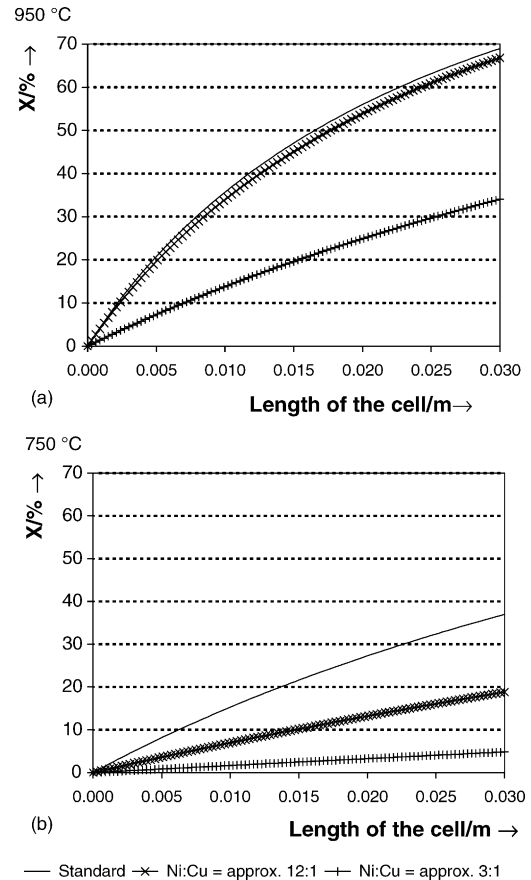

Fig. 9. By means of the determined kinetic constants calculated methane conversion along the length of one single cell for 950 °C (a) and 750 °C (b). Anode: $\dot{V}_{0,CH_4,SATP} = 17.641 \, h^{-1}$, $\dot{n}_{0,H_2O}/\dot{n}_{0,CH_4} = 2$, $x_{0,H_2} = 0.02$.

reaction rate down to almost 30%. At 750 °C the reforming rate constant diminishes even by a factor of 10.

In order to illustrate these findings Fig. 9 shows the calculated conversion in flow direction along the length of the anode for a temperature of 950 °C (a) and 750 °C (b). The differences between the three curves for case (a) and (b) make clear that the activation energy increases with higher copper content and the reaction rate declines.

By subsequently impregnating ready made standard cells the amount of copper that can be introduced is limited. Once the amount becomes too high the distribution of copper over the cross-section of the anode may start to become uneven

and a porosity decrease of the cermet may be expected as well. Due to the limited amount of standard cells available for this study, these effects could not yet be quantified. Up to a copper to nickel ratio of $0.5 \, kg_{Cu} \, kg_{Ni}^{-1}$, obviously no negative effects are encountered that would lower the electrochemical activity significantly. It is not yet clear at what point concerning the copper content the minimum reforming activity would be reached. Measurements by X-ray photoelectron spectroscopy on the modified anodes as well as published data [13,20,21] point out that at higher temperatures as they occur in SOFC operation, the surface is probably enriched

Table 1
Comparison of the derived kinetic constants for methane steam reforming on the standard Ni–YSZ cermet and different modified anode materials

	Standard	Ni:Cu = 12:1	Ni:Cu = 3:1
k_1^*	$-1.2 \times 10^{+01} \pm 4.9 \times 10^{-02}$	$-1.3 \times 10^{+01} \pm 3.1 \times 10^{-02}$	$-1.4 \times 10^{+01} \pm 7.8 \times 10^{-02}$
E_1^*	$7.1 \times 10^{+00} \pm 1.1 \times 10^{-03}$	$1.2 \times 10^{+01} \pm 7.0 \times 10^{-02}$	$1.4 \times 10^{+01} \pm 6.6 \times 10^{-02}$
$k_{0,1}$ (mol^{-1} m^{-2} s^{-1} Pa^{-1})	4.98×10^{-03}	2.61×10^{-01}	6.76×10^{-01}
$E_{A,1}$ (J^{-1} mol^{-1})	$6.33 \times 10^{+04}$	$1.04 \times 10^{+05}$	$1.25 \times 10^{+05}$
$k_{1,950 °C}/k_{1,standard,950 °C} \times 100$ (%)	100.0	93.6	31.6
$k_{1,850 °C}/k_{1,standard,950 °C} \times 100$ (%)	57.5	37.6	10.6
$k_{1,750 °C}/k_{1,standard,950 °C} \times 100$ (%)	29.6	12.6	2.9
$k_{1,650 °C}/k_{1,standard,950 °C} \times 100$ (%)	13.2	3.3	0.6

with copper. As the diffusion processes in the alloy phase strongly depend on temperature and probably also rely on the gas phase composition, it is difficult to quantify the actual composition on the anode surface under reaction conditions, which should be directly related to the changes in the reaction rates.

The kinetic constants determined in this work are effective reaction constants, which apply only to the type of anode used in this investigation. The question remains whether the porous structure of the anode has a significant influence on the reaction rates. There might be limiting diffusion processes within the pores of the anode layer which could be partly responsible for the observed change of the reaction rates. Thus, a more detailed modelling is necessary to determine more exactly the influence of the modification by copper on the intrinsic kinetic performance of the anode.

To increase the life time and to allow cost reduction, a lower operation temperature of solid oxide fuel cells is favourable. To achieve this objective the cell resistance has to be lowered, e.g. by using an electrode-supported cell design with a thin electrolyte layer. A concept which is proposed by many researchers is the upcoming anode-supported cell with an operation window of 650–850 °C. In general, a decreasing temperature leads to smaller temperature gradients. On the other hand the reforming reaction is still much faster than the oxidation reaction and the thick anode (0.5–2 mm) lacks good heat conduction ability. Therefore, the impregnation with copper could be a helpful tool to lower the high amount of surface nickel atoms in such an anode and improve the cell performance when using methane as fuel [22–24].

Several researchers already ascertained the favourable influence of copper on the problem of carbon formation [13,14,21]. In this investigation coking was neglected as the focused operating conditions include a sizeable amount of steam excess. For the commercialisation of fuel cells it would be advantageous to use fuels, which are not fully utilised by conventional power generators. Biogas could provide such a niche for the new technology. This fuel, however, is more likely to cause carbon deposition on the anode. Thus, it is of great interest to investigate the effect of copper also when the feed gas is varied.

4. Conclusions

The developed wet impregnation procedure is a reliable, economical method for coating the standard Ni–YSZ cermets with copper. EPMA measurements revealed a constant ratio of copper to nickel over the thickness of the anode as well as a relatively even distribution of copper over the surface area of the anode. A ratio up to 0.3–0.5 $kg_{cu}\,kg_{Ni}^{-1}$ could be reached with this method. Current density–voltage characteristics proved that it is possible to maintain an electrochemical performance comparable to that of the standard cells. The comparison of the reforming activity was based on measurements without load to avoid an influence of the nickel mesh used to contact the anode when there was a current flow. The catalytic activity for the steam reforming reaction diminishes strongly with rising copper content. A copper to nickel ratio of 1:3 caused a decrease of the reforming rate constant at 950 °C by a factor of 3, at 750 °C by a factor of 10. Therefore, the catalytic modification with copper is considered to be a promising technique for improving the performance of hydrocarbon-fuelled solid oxide fuel cells. In combination with chemical engineering measures it could enable the direct conversion of natural gas and steam in the anode chamber without the necessity of pre-reforming.

References

[1] B.C.H. Steele, Nature 400 (1999) 619–621.
[2] R. Peters, E. Riensche, P. Cremer, J. Power Sources 86 (2000) 432–441.
[3] E. Riensche, VDI Berichte 1174 (1995) 63–78.
[4] S.H. Clarke, A.L. Dicks, K. Pointon, T.A. Smith, A. Swann, Catal. Today 38 (1997) 411–423.
[5] R. Peters, R. Dahl, U. Klüttgen, C. Palm, D. Stolten, J. Power Sources 106 (2002) 238–244.
[6] R. Fellows, J. Power Sources 71 (1998) 281–287.
[7] A.L. Dicks, J. Power Sources 71 (1998) 111–122.
[8] J. Schüle, H. Ringel, Forschungszentrum Jülich GmbH, Patent DE 101 26 723 A 1, 2001.
[9] B.C.H. Steele, Solid State Ionics 86–88 (1996) 1223–1234.
[10] A.-L. Sauvet, J. Foultier, J. Power Sources 101 (2001) 259–266.
[11] K. Morimoto, M. Shimotsu, in: M. Dokiya, O. Yamamoto, H. Tagawa, S.C. Singhal (Eds.), Solid Oxide Fuel Cells IV, vol. 95-1, The Electrochemical Society Proceedings Series, Pennington, NJ, 1995, pp. 769–778.
[12] S. Onuma, A. Kaimai, K. Kawamura, Y. Nigara, T. Kawada, J. Mizusaki, H. Inaba, H. Tagawa, in: U. Stimming, S.C. Singhal, H. Tagawa, W. Lehnert (Eds.), Solid Oxide Fuel Cells V, vol. 97-40, The Electrochemical Society Proceedings Series, Pennington, NJ, 1997, pp. 483–490.
[13] J.H. Sinfelt, J.L. Carter, D.J.C. Yates, J. Catal. 24 (1972) 283–296.
[14] C.A. Bernardo, I. Alstrup, J.R. Rostrup-Nielsen, J. Catal. 96 (1985) 517–534.
[15] M.E.S. Hegarty, A.M. O'Connor, J.R.H. Ross, Catal. Today 42 (1998) 225–232.
[16] M.S. Spencer, Catal. Today 12 (1992) 453–464.
[17] S. Park, R.J. Gorte, J.M. Vohs, Appl. Catal. A: Gen. 200 (2000) 55–61.
[18] L. Zanibelli, C. Flego, C. Perego, in: U. Bossel (Ed.), Proceedings First European Solid Oxide Fuel Cell Forum, Luzern, Schweiz, 1994, pp. 207–216.

[19] A.L. Dicks, K.D. Pointon, A. Siddle, J. Power Sources 86 (2000) 523–530.

[20] I. Alstrup, U.E. Petersen, J.R. Rostrup-Nielsen, J. Catal. 191 (2000) 401–408.

[21] H. Kim, C. Lu, W.L. Worrell, J.M. Vohs, R.J. Gorte, J. Electrochem. Soc. 149 (2002) A247–A250.

[22] T. Ackmann, L.G.J. de Haart, W. Lehnert, D. Stolten, J. Electrochem. Soc. 150 (2003) A783–A789.

[23] J.-H. Koh, Y.-S. Yoo, J.-W. Park, H.C. Lim, Solid State Ionics 149 (2002) 157–166.

[24] Y.J. Leng, S.H. Chan, K.A. Khor, S.P. Jiang, Int. J. Hydrogen Energy 29 (2004) 1025–1033.